Journal of Hazardous Materials 333 (2017) 80–87

Contents lists available at ScienceDirect

Journal of Hazardous Materials

journal homepage: www.elsevier.com/locate/jhazmat

Insight into highly efficient co-removal of *p*-nitrophenol and lead by nitrogen-functionalized magnetic ordered mesoporous carbon: Performance and modelling

Yaoyu Zhou[a,b], Xiaocheng Liu[a], Lin Tang[b,c,*], Fengfeng Zhang[a], Guangming Zeng[b,c], Xiangqi Peng[a], Lin Luo[a], Yaochen Deng[b,c], Ya Pang[d], Jiachao Zhang[a]

[a] College of Resources and Environment, Hunan Agricultural University, Changsha 410128, China
[b] College of Environmental Science and Engineering, Hunan University, Changsha 410082, China
[c] Key Laboratory of Environmental Biology and Pollution Control, Hunan University, Ministry of Education, Changsha 410082, China
[d] Department of Biotechnology and Environmental Science, Changsha College, Changsha 410003, China

HIGHLIGHTS

- Efficient Pb(II) and *p*-nitrophenol adsorption on N-Fe/OMC.
- The mutual competition and enhancement of their mutual interaction were revealed.
- Modelling of Pb(II) and PNP removal by taking into account sorption processes.
- Give new insights on the development of OMC materials and advances its applications.

GRAPHICAL ABSTRACT

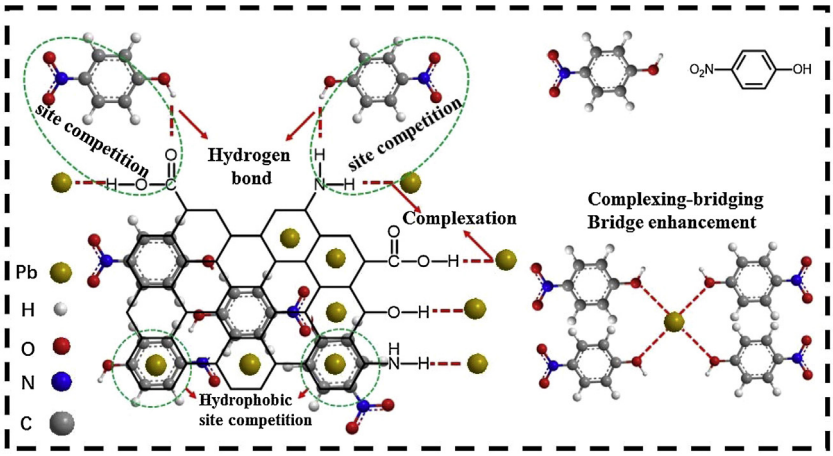

ARTICLE INFO

Article history:
Received 1 November 2016
Received in revised form 26 February 2017
Accepted 13 March 2017
Available online 16 March 2017

Keywords:
Lead
p-nitrophenol
Sorption
Ordered mesoporous carbon
Modelling

ABSTRACT

Highly efficient simultaneous removal of Pb(II) and *p*-nitrophenol (PNP) contamination from water was accomplished by nitrogen-functionalized magnetic ordered mesoporous carbon (N-Fe/OMC). The mutual effects and inner mechanisms of their adsorption onto N-Fe/OMC were systematically investigated by sole and binary systems, and thermodynamic, sorption isotherm and adsorption kinetics models. The liquid-film diffusion step might be the rate-limiting step for PNP and Pb(II). The fitting of experimental data with Temkin model indicates that the adsorption process of PNP and Pb(II) involve physisorption and chemisorption. There exist site competition and enhancement of PNP and Pb(II) on

* Corresponding author at: College of Environmental Science and Engineering, Hunan University, Changsha 410082, China.
E-mail addresses: tanglin@hnu.edu.cn, etanglin@gmail.com (L. Tang).

http://dx.doi.org/10.1016/j.jhazmat.2017.03.031

the sorption to N-Fe/OMC. Moreover, N-Fe/OMC could be regenerated effectively and recycled by using dilute NaOH and acetone. These demonstrated superior properties of N-Fe/OMC indicate that it could be applied to treatment of wastewaters containing both lead and PNP.

1. Introduction

Recalcitrant organic compounds and inorganic pollutants such as nitroaromatic compounds and heavy metals are common in the real environment, hence, giving rise to a serious damage to human health and the ecosystem. For example, *p*-nitrophenol (PNP), a hydrolytic product from the degradation of organophosphorus pesticides, may cause serious harm to human health because of its mutagenic potential and the possible damage on kidney and liver [1,2]. Heavy metals, such as lead, released from industrial operations such as agricultural industries and metal plating/coating, cause toxic effect even at trace concentration in humans (e.g., neurological, cardiovascular, reproductive, and developmental disorders) [3–6].

The co-existence of nitroaromatic compounds and heavy metals may occur as complex solute mixtures in contaminated water and soil, and pose more serious toxicological problems to the environment because of their relative mobility and combined toxicity [7]. For example, PNP and Pb may exist together in wastewater from agricultural irrigation [8,9]. Therefore, finding effective ways to control these combined pollutants has aroused continuous concern recently.

Various methods (e.g., adsorption, advanced oxidation, electrochemical methods, chemical precipitation, biological treatment and membrane treatment) have been extensively applied to remove recalcitrant organic compounds and/or heavy metals with a positive effect in aqueous solution previously [10–15]. Among these treatment methods, the adsorption technology was a priority choice because of a synthetic consideration of economic feasibility, removal efficiency, the simplicity and safety of the treatment process [16–18]. Furthermore, various adsorbents such as polyamine chelating resin [8], biosorbents[19], na-montmorillonite [20], mauritanian clay [21], and etc. have been applied to remove the coexisting pollutants of heavy metal and nitroaromatic compounds [20,22,23]. For examples, Chen et al. [8] applied polyamine chelating resin to adsorb *p*-nitrophenol and copper with high efficiency, and clarified co-existed pollutants competition and enhancement effect upon site recognition. Ristori et al. [20] and Abdelhahi et al. [21] used the mauritanian clay to remove copper and nitrophenol simultaneously, and investigated the competitive adsorption between copper and nitrophenol.

Moreover, searching for new efficient, simple, recycled, regenerated and inexpensive methods to control heavy metals and recalcitrant organic compounds is also of considerable interest. Nowadays, the utilization of carbon-based materials (e.g., carbon nanotubes, graphene, mesoporous carbon) as a high efficient adsorbent (e.g., controlled pore size distribution, high surface area to volume ratio and manipulatable surface chemistry) for pollution remediation (recalcitrant organic compounds and/or heavy metals) was drawing more and more attention [7,24]. For examples, Zhou et al. [25] developed carbon nanotubes/$CoFe_2O_4$ magnetic hybrid material (an efficient, eco-friendly and reusable adsorbent) with high specific surface area and abundant functional groups for the removal of tetrabromobisphenol A and Pb(II). Gao et al. [26] synthesized polydopamine-functionalized graphene hydrogel as reusable adsorbents for removal of heavy metals, synthetic dyes, and aromatic pollutants.

In addition, ordered mesoporous carbons (OMCs), one of carbon-based materials, were introduced as candidates in pollutant removal by researchers for the following reasons: i) OMCs possess intrinsic high specific surface areas, regular and tunable pore sizes, large pore volumes, enabling the possibility of physisorption and hydrophobic interaction and electrostatic adsorption with pollutants efficiently [27]. ii) OMCs possess stable and interconnected frameworks with active pore surfaces for modification or functionalization, enabling the possibility of specific binding (e.g., hydrogen bonding, van der Waals interactions as well as covalent binding) for contaminants efficiently [28]. Hence, to enhance the adsorption effect of pristine OMCs, the modification of OMC was essential to improve its surface properties, such as effective functional groups, hydrophobic/hydrophilic property, or surface charge [29]. And the most popular reagents which are used for oxidation/functionalization of OMC surface include nitric acid [30], ammonium persulfate [31], aminopropyltriethoxysilane [29], and ethylenediamine[32]. For examples, Barczak et al. [29] reported amino-functionalized OMC (treated with aminopropyltriethoxysilane) for the removal of heavy metal ions (Pb, Zn, Cu, Cd) from the aqueous solutions. Chen et al. [32] used a functionalized OMC (treated with nitric acid and thionyl chloride) for the selective adsorption of Cu(II) and Cr(VI).

Recently, we synthesized polyacrylic acid modified magnetic OMC, iron oxide nanoparticles-doped carboxylic OMC, cobalt nanoparticles-embedded magnetic OMC, nonmetal atoms of N and P doped OMC, and used for the effective removal of recalcitrant organic compounds and heavy metals from wastewater [18,33–36]. Previous work indicated that the surface and physicochemical properties of OMC can be easily modified with functional groups or incorporated with transition metal (Fe and Co) and heteroatoms (N, B, and S), exhibiting improved physical or chemical properties for the removal of hazardous contaminants.

In this work, we focused our efforts on the following: (1) demonstration of the adsorption ability of the prepared nitrogen-functionalized magnetic ordered mesoporous carbon (N-Fe/OMC) for Pb(II) and *p*-nitrophenol simultaneously, (2) investigation of the impacts of some key parameters, namely pH, contact time and temperature on the adsorption capacity; (3) modelling of adsorption isotherms, kinetics and thermodynamics were analyzed to help explain its adsorption mechanism of Pb(II) or *p*-nitrophenol, (4) investigation of the underlying mechanisms of Pb(II) and *p*-nitrophenol adsorption onto N-Fe/OMC. This study provides new insights in the development of mesoporous carbon materials and advances their applications in water treatment.

2. Materials and methods

2.1. Reagents

Pluronic copolymer P123 ($EO_{20}PO_{70}EO_{20}$, EO = ethylene oxide, PO = propylene oxide) was purchased from Sigma-Aldrich (USA). $Pb(NO_3)_2{\cdot}3H_2O$, $Fe(NO_3)_3{\cdot}9H_2O$, oxalic acid, furfuryl alcohol, alcohol, *p*-nitrophenol and all other reagents were analytical-grade and were used as received without further purification. High-purity water (18.25 MΩ/cm) from a Millipore Milli-Q water purification system was used in all experiments.

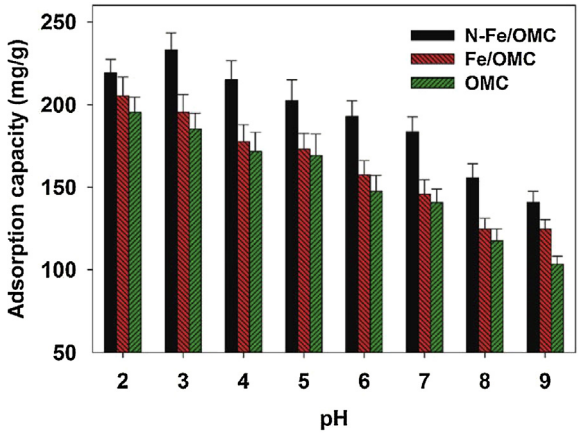

Fig. 1. Adsorption amounts for PNP onto OMC, Fe/OMC, N-Fe/OMC from single systems, initial PNP concentration of 150 mg/L, at 25 °C.

2.2. Preparation and characterization of N-Fe/OMC

The mesostructured SBA-15 silica template was synthesized as described previously in our laboratory [7,37,38]. Besides, Fe/OMC and N-Fe/OMC was synthesized as described previously in our laboratory [39]. Details about the preparation of Fe/OMC and N-Fe/OMC can be seen in Supporting Information (SI). The zeta potential of N-Fe/OMC was determined by using Electroacoustic Spectrometer (ZEN3600 Zetasizer UK) at varying solution pH from 2.0 to 7.0, and the result was presented in Fig. S-1. Furthermore, the structural information for N-Fe/OMC including SEM and TEM were presented in Fig. S-2. The Fourier-transform infrared (FT-IR) spectrum, X-ray powder diffraction (XRD), magnetic data and N_2 sorption isotherms with the corresponding pore distribution curves were described in our previous work, indicating that the N-Fe/OMC was enriched with amino and oxygen-containing functional groups [7]. The amino group, oxygen-containing functional group and numerous pores on the outside of the OMC implied that N-Fe/OMC contained both hydrophilic and hydrophobic sites [7].

2.3. Mathematical modelling

The pseudo-first-order, pseudo-second-order model, two-compartment first-order model, intra-particle diffusion model and Boyd model were applied to fit the experiment data respectively, and the equations were presented in Text S-2. The Langmuir, Freundlich isotherm, Temkin and Dubinin–Radushkevich models presented in Text S-3 were used to investigate the reaction behavior between the target molecules and the solid material. In addition, the model parameters have been determined by the derivative of marquardt's percent standard deviation (MPSD). A minimization procedure has been adopted to solve kinetic equations by minimizing the sum of squared error (SSE), and the equations were presented in Text S-4.

3. Results and discussion

3.1. The sole systems for PNP

3.1.1. Effect of solution pH

The effect of initial solution pH on the removal of PNP with OMC, Fe/OMC, and N-Fe/OMC were investigated by varying the solution pH from 2.0 to 9.0, and the results were presented in Fig. 1. It can be seen that the overall trend of the impact of initial solution pH on PNP adsorption was similar using these OMC-based materials. The PNP adsorption decreased with the increased solution pH. Besides, the adsorption capacities for PNP were in the following order: N-Fe/OMC > Fe/OMC > OMC. N-Fe/OMC exhibited the highest adsorption capacity. This was probably because N-Fe/OMC provided a higher specific surface area and numerous pores, thus there exist enough hydrophobic sites for the sorption of PNP by hydrophobic interactions and physical absorption [8,40].

Besides, a larger number of amino, carboxyl and hydroxyl groups in N-Fe/OMC may offer additional affinity and more available binding sites, and thus through hydrogen bond between the hydroxyl groups in PNP molecules and amino, hydroxyl or carboxyl groups on N-Fe/OMC surface for PNP removal. Furthermore, the molecule of PNP consists of the aromatic ring including the functional groups of —OH (electron donor) and —NO_2 (electron acceptor), and thus, the small amount of oxygen-containing groups on the surface of N-Fe/OMC and the electron acceptor —NO_2 in PNP decreased the electron density of the basal planes and aromatic ring, leading to a weaker π-π dispersion interaction.

In addition, the electrostatic repulsion/interaction between PNP and N-Fe/OMC were also investigated though zeta potential measurement of N-Fe/OMC (Fig. S-1). In acid solution (pH from 2.0 to 7.0), the PNP was mainly in molecules form whose pK_a value was 7.15, and the adsorption of PNP may be ascribing to the hydrophobic interaction, hydrogen bond, physical absorption, and π-π dispersion interaction [41,42]. In alkaline solution, the surface of the material was deprotonated because of pH > pH_{zpc}, and a larger portion of PNP was ionized. It could be found that a sharp decrease of PNP adsorption amount from pH 7.0–9.0 resulted from the electrostatic repulsion, which played a vital role in the reaction between the ionized PNP and adsorbent with negatively charged surface.

Furthermore, it could be observed that the N-Fe/OMC obtained the maximum adsorption capacity for PNP at pH 3.0, and thus other experiments to perform PNP removal by the material were conducted at pH 3.0.

3.1.2. Effect of contact time and adsorption kinetics

The effect of reaction time on PNP removal by OMC-based materials was conducted at pH 3.0 and 25 °C using 150 mg/L PNP, and the results was present in Fig. S-3. It was noteworthy that the removal rate of PNP by N-Fe/OMC was the fastest among these materials, and the removal of PNP rapidly occurred in the first 120 min accounted for 80% of the total adsorption capacity, followed by a slower adsorption process until it reached equilibrium at 200 min.

The pseudo-first-order and pseudo-second-order models are often used to investigate the adsorption kinetics [43–45], and the equations were presented in Text S-2. The calculated results of first-order and second-order rate equations are shown in Table S-1. The correlation coefficient (R^2) and the sum of error squared (SSE) suggested that the pseudo-second-order model (R^2 = 0.9979–0.9995) fitted with the experimental data better in comparison to the pseudo-first-order model (R^2 = 0.8000–0.8896). Meanwhile, the adsorption capacity calculated from pseudo-second-order equation (SSE = 0.422–0.856) was more consistent with the experimental Q_e (mg g^{-1}) value than that calculated from the pseudo-first-order model (SSE = 10.46–15.33) (Fig. S-4). The plots of t/Q_t versus t for the pseudo-second-order equation are shown in Fig. 2A. Thus, the experimental results supported the assumption based on the pseudo-second-order model that the mechanism of PNP adsorption was chemisorption which involved valency forces through sharing or exchanging electrons between the N-Fe/OMC and PNP. Furthermore, the constant k_2 calculated from the pseudo-second-order model was used to calculate the initial sorption rate h (mg g^{-1} min^{-1}), at t → 0, and the equations were presented in Text S-2. And the results were shown in Table S-1, it is revealed that the initial sorption rate of N-Fe/OMC is the fastest compared to Fe/OMC and OMC.

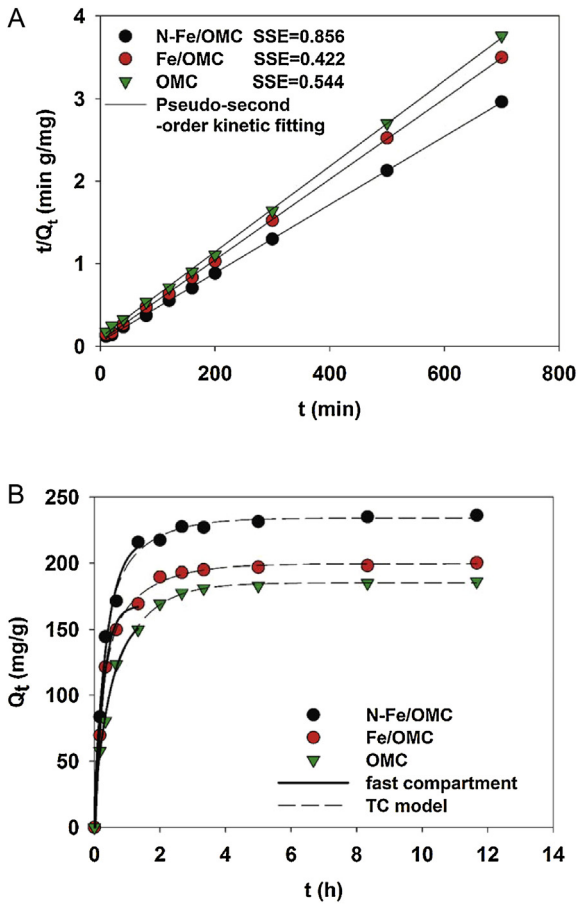

Fig. 2. Kinetics of PNP sorption onto OMC-based materials by fitting two-compartment (TC) model, and pseudo-second-order model.

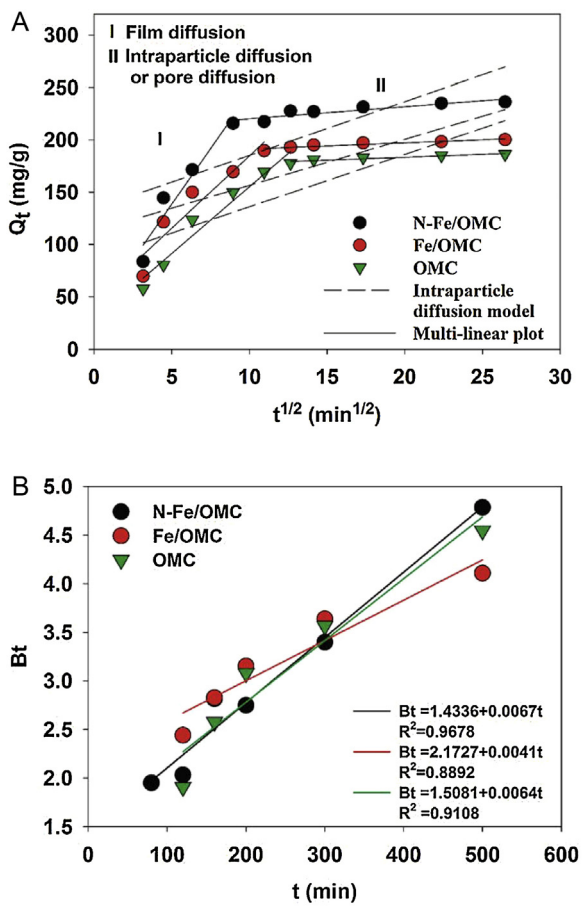

Fig. 3. Intra-particle diffusion contact time on PNP adsorption (A), and Boyd plots for the adsorption of PNP onto the OMC-based materials. Initial PNP concentrations of 150 mg/L, adsorbents dose of 5 mg, pH 3.0, temperature of 25 °C.

Besides, the time-courses of PNP sorption onto OMC-based materials were analyzed with a two-compartment first-order model, and its equation was presented in Text S-2. The result was depicted in Fig. 2B. It could be seen that two-compartment model considered the adsorption of PNP by OMC-based materials as a two-domain process. As shown in Table S-1, the TC model well fitted the dynamics data of PNP adsorption on OMC, Fe/OMC and N-Fe/OMC with R^2 ranged in 0.9903-0.9974. The F_{fast} value of OMC-based materials were greater than those of F_{slow}, indicating that the fast sorption stage was predominant during PNP sorption process. As can be seen in Fig. 2B, during a relatively short contact time, such as 80 min, the fast compartment achieved 91.36%, 84.62% and 80.45% of their own sorption capacity of N-Fe/OMC, Fe/OMC and OMC, respectively, while the rest of the sorption capacity was contributed by slow compartment between 80 min to 700 min. The k_{fast} value for PNP were in the following order: N-Fe/OMC > Fe/OMC > OMC, indicating that N-Fe/OMC provided more active for PNP in the removal process. It is commonly considered that the hydrogen bond between the hydroxyl groups in PNP molecules and amino, hydroxyl or carboxyl groups on N-Fe/OMC surface as well as the electrostatic interaction are responsible for the fast sorption of PNP and may reach equilibrium in a short period.

When the sorbent is mixed with PNP solution, predicting the rate-limiting step during the transport of the PNP from the solution through the interface of solution/sorbent and into the particle pores in sorbent is another important issue to be considered. Generally, the sorption process of a sorbate by a porous sorbent can be classified as three consecutive steps: (i) mass transfer across the external boundary layer film of liquid surrounding the outside of the particle (external diffusion or film diffusion); (ii) diffusion from the surface to the intraparticular sites (intraparticular diffusion or pore diffusion); and (iii) adsorption at an active site on the external or internal surface of sorbent. The third step is often considered to be extremely rapid, thus the most dominant steps for adsorption are film or/and pore diffusion [46–48].

In order to determine whether the actual rate-controlling step results from film diffusion or pore diffusion, the kinetic data have been analyzed using the intraparticle diffusion model and Boyd model, which is presented in Text S-2. As seen in Fig. 3A, it was quickly evident that the plot of Q_t vs. $t^{1/2}$ of OMC-based materials was multi-linear, indicating that the sorption was affected by more than one process. Besides, it could be speculated that the adsorption processes of the three elements occurred in two phases, indicating that the intra-particle diffusion was not the rate-limiting step during the whole process [49]. And the initial portion of the plot may indicated an external diffusion or film diffusion, while the second linear portion was caused by intra-particle or pore diffusion [50]. Similar results have been reported by Dehghani et al. using single-walled and multi-walled carbon nanotubes for the removal of phenol [51].

In addition, the linearity plot of Bt vs. time plots was also employed to distinguish between sorption controlled by film diffusion or particle diffusion. If a plot of *Bt* vs. time (having slope B) is a straight line passing through the origin, then the sorption is governed by a particle diffusion mechanism; otherwise, it is governed by film diffusion. In fact, it is impossible to find exact values of Bt in Eq. (10) as it is implicit with respect to parameter Bt; it is possible to find highly accurate approximates of Bt by solving the nonlinear transcendental Eq. (10) by means of the Adomian decomposition

method[52–55]. Here, with the values of F from 0.86 to 1, Bt was calculated by Eq. (10) in Supporting information according to proposed method by Reichenberg et al. [56]. As seen in Fig. 3B, the plots of OMC-based sorbents illustrated that the fitted lines don't pass through the origin, indicating the film-diffusion-controlled mechanism.

Therefore, as described from these models, the kinetics of interaction of PNP with the OMC-based materials surfaces are not overwhelmingly controlled by any one mechanism. Although the film-diffusion-controlled mechanism is more likely to dominate, contributions from pore diffusion could not be completely ruled out.

3.1.3. Sorption isotherm and thermodynamic studies

The adsorption isotherms studies were used to investigate the reaction behavior between the PNP molecules and the solid material. The distribution of the PNP between the solution and adsorbent phase is a criterion of the adsorbate-adorbent balance in the adsorption process, and expressed by one of several adsorption isotherm models. Some well-known ones are Langmuir, Freundlich, Temkin, Dubinin-Radushkevich, Redlich-Peterson and Sips [2,57,58]. These models are applied to assist interpreting the mechanism.

Herein, the Langmuir, Freundlich, Temkin and Dubinin-Radushkevich isotherm models were used to fit the experiment data respectively, which is presented in Text S-3. The Langmuir isotherm model is set up based on the hypothesis that a monomolecular layer is formed, and adsorption takes place without any interaction between the adsorbed molecules, representing the monolayer adsorption of adsorbate molecules on homogeneous adsorbent active sites [57]. The Freundlich isotherm model describes that the binding sites were not equal and the adsorption takes place with a heterogeneous surface from extensive experience [57]. The Temkin isotherm contains a factor that indicated the interactions between the adsorbent and the adsorbed particles, and the Dubinin-Radushkevich model was used to determine the nature of biosorption processes as physical or chemical [2]. The equations are expressed in Text S-3.

In addition, the separation factor (R_L), defined by Hall et al. [58], which based on the Langmuir model was used to evaluate the adsorption process, and it was defined in Text S-3. In order to determine the maximum sorption capacity by Freundlich isotherm model, it is necessary to operate with constant initial concentration C_0 and variable weights of sorbent, the calculated method was described by Halsey [59], which is presented in Text S-3.

Moreover, the model parameters for these three isotherm have been determined by minimizing the difference between the experimental and modeled Q_e values (through the derivative of MPSD) using the iterative method [60], which is presented in Text S-3.

The results of the relevant parameters calculated from the above three isotherm models were shown in Figs. 4 and S-5. It was evident that comparing with the Freundlich model and Dubinin-Radushkevich model, the Langmuir model and Temkin model fitted the experiment data better in view of its higher correlation coefficient (R^2). Besides, the Langmuir model and Temkin model showed lower values of the derivative of MPSD. For Langmuir model, it suggested that the homogeneous adsorption of PNP occurred on the adsorbent. Furthermore, as seen in Fig. 4A, while $K_L > 0$, the value of separation factor R_L was 0.02193, so the adsorption process is favorable at operation condition. The low R_L value (<0.04) demonstrates that the interaction between PNP and N-Fe/OMC is relatively strong [61]. As for Temkin model, typical physisorption processes are reported to have adsorption energies less than −40 kJ mol^{-1}, while bonding energy range for ion-exchange mechanism is reported to be in the range of 8–16 kJ mol^{-1} [62]. In the present study, values of b_T at the initial temperature of 25 °C was 0.04865 kJ mol^{-1}, indicating that the adsorption process may involve physisorption and chemisorption. In addition, as presented in Table S-4, it can be seen that N-Fe/OMC showed a relatively high sorption capacities for PNP in comparison with other adsorbents.

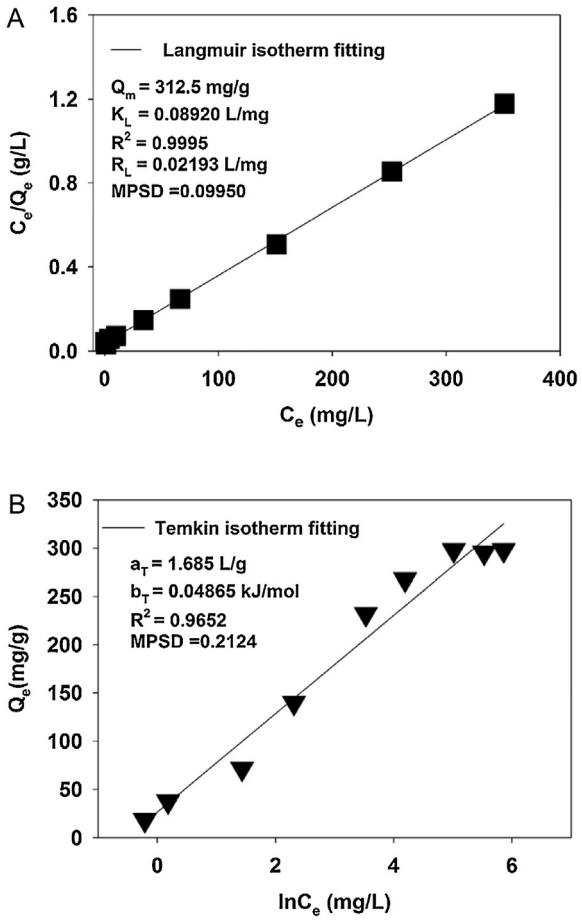

Fig. 4. The Langmuir and Temkin isotherm model isothermal (A and B) fittings for PNP adsorption on N-Fe/OMC.

The adsorption thermodynamic studies were conducted at 298.15 K, 308.15 K, and 318.15 K, respectively to evaluate the adsorption reaction. Three thermodynamic parameters, the enthalpy change (ΔH, kJ/mol), the free energy change (ΔG, kJ/mol) and the entropy change (ΔS, kJ K^{-1} mol^{-1}) were determined by the equations listed in Text S-5. The result was depicted in Table S-2. It could be seen that ΔG values towards PNP adsorption was negative, indicating that the uptake of PNP was spontaneous at these temperatures. The positive ΔH confirmed the endothermic nature of adsorption. Besides, the positive values of ΔS implies an increasing randomness during the adsorption process.

3.2. The single system for Pb(II) adsorption

In order to obtain the adsorption mechanism for Pb(II) by N-Fe/OMC, and the essential adsorption characteristics, the batch experiments for Pb(II) adsorption were conducted to find out the effect of solution pH and its adsorption isotherm type.

Adsorption of Pb(II) on N-Fe/OMC, Fe/OMC and OMC at different pH were presented in Fig. S-6. In order to avoid the precipitation of Pb(II), the experiments were conducted for Pb(II) adsorption with solution pH range from 2.0 to 6.0. It could be observed that the adsorption capacity for Pb(II) by OMC-based materials was increased with the pH from 2.0 to 6.0. The Pb(II) adsorption capacities, except for the pH of 4.0, were in the following order:

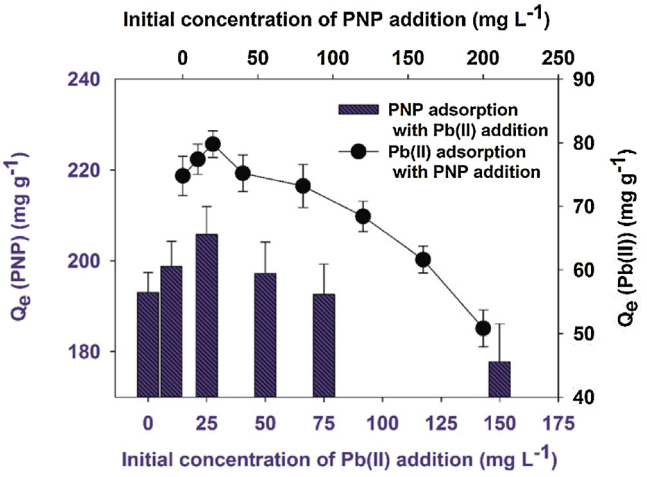

Fig. 5. The PNP (150 mg L^{-1}) adsorption with Pb(II) addition (0–150 mg L^{-1}); and the Pb(II) (50 mg L^{-1}) adsorption with PNP addition (0–200 mg L^{-1}).

N-Fe/OMC > Fe/OMC > OMC, indicating that the Fe doped OMC and nitrogen atoms incorporation enhanced adsorption capacity of OMC. Specifically, in the preparation process of the doped OMC by iron oxide nanoparticles, the oxygen atoms were provided on the surface of OMC [63], and amino groups were introduced to the doped OMC, which chelated strongly with targeted Pb(II) [7].

However, the N-Fe/OMC showed lower adsorption capacity for Pb(II) at pH 4.0 which might result from its pH_{zpc}. The pH_{zpc} of the Fe/OMC was 3.54, while N-Fe/OMC was 4.76, when the solution pH was 4.0, electrostatic attraction generated between the cationic Pb(II) and the negatively charged adsorbents of Fe/OMC was beneficial for Pb(II) adsorption.

As shown in Fig. S-7, the adsorption type of Pb(II) adsorption onto N-Fe/OMC could be well described by the Langmuir isotherm model ascribing to its higher correlation coefficient (R^2 = 0.9983) and lower values of MPSD as 0.1833, indicating the monolayer adsorption for Pb(II) on the adsorbent, and it was consistent with the result obtained by the previous research [7]. Although the model of Temkin did not exactly show the higher correlation coefficient (R^2 = 0.9360) and lower values of the MPSD, the values of b_T at the initial temperature of 25 °C was 0.0929 kJ mol^{-1}, indicating that the adsorption process seems to involve physisorption and chemisorption. In addition, the N-Fe/OMC showed a relatively high sorption capacities for Pb(II) in comparison with other adsorbents (Table S-4).

As shown in Figs. S-8 and S-9, the kinetics of interaction of PNP with the N-Fe/OMC surfaces are more likely controlled by the second-order mechanism and film-diffusion-controlled mechanism compared to the first-order as well as pore diffusion. And the results from the adsorption kinetics of PNP and Pb(II) indicated that PNP and Pb(II) may have the similar adsorption process, and may exist the site competition between them. Therefore, it is very necessary to investigate the adsorption of Pb(II) and PNP onto sorbent simultaneously.

3.3. The binary systems for Pb(II) and PNP

To evaluate the effect of the simultaneous existance of PNP and Pb(II) on their mutual adsorption onto N-Fe/OMC, the binary adsorption experiments were conducted by varying PNP or Pb(II) concentration with another one fixed at pH 6.0, and the results were shown in Fig. 5. I It could be observed that the presence of Pb(II) at 10 mg/L, 25 mg/L, respectively could slightly promote the PNP adsorption by comparison with the single PNP adsorption system with no Pb(II) addition, and the promoted PNP adsorption might be ascribed to the formed PNP-Pb(II) complex. Furthermore, under the same initial PNP concentration, the PNP adsorption capacity decreased when the coexisting Pb(II) concentration increased from 25 to 75 mg/L. It indicated that the complexation interaction between Pb(II) and PNP occurred only in a small portion, and greater competitive adsorption between them for adsorption sites on N-Fe/OMC existed at higher Pb(II) concentration. While the concentration of Pb(II) was high than 75 mg/L, the competitive adsorption between them predominated, and the PNP adsorption was suppressed. Similar results have been reported by Tang's group [7] and Chen et al. on various adsorbents [64].

The influence of coexisting PNP on the adsorption capacity of Pb(II) onto N-Fe/OMC was indicated based on the Pb(II) adsorption capacity with PNP addition (0–200 mg L^{-1}). From Fig. 5, it could be observed that when Pb(II) was 50 mg/L, the coexisted low concentration of PNP (from 10 to 20 mg/L) could slightly facilitate the Pb(II) adsorption. However, the promoted adsorption was not obvious when the PNP increased to 80 mg/L. With the further increase of coexisting PNP concentration, the growing residual Pb(II) concentration in solution indicated the suppressed Pb(II) adsorption on N-Fe/OMC by PNP.

3.4. Mechanism analysis for PNP and Pb(II) adsorption

The adsorption mechanism for PNP and Pb(II) adsorption onto N-Fe/OMC was proposed based on all information obtained above. From their single adsorption system conducted above, it could be deduced from Temkin model that the adsorption process of PNP involve physisorption and chemisorption, indicating that the PNP was adsorbed mainly by hydrophobic sites (physisorption) and hydrogen bonding (chemisorption) on N-Fe/OMC. And Pb(II) might be mainly adsorbed by the amino groups and oxygen-containing groups of hydrophilic sites (chemisorption) and porous structure of the adsorbent (physisorption). The results indicated that PNP and Pb(II) might have the same adsorption sites. Therefore, it was initially expected that the site competition between PNP and Pb(II) during their adsorption onto N-Fe/OMC, thus decreasing their sorption. However, the coexisted low concentration of PNP (from 10 to 20 mg/L) or Pb(II) (from 10 to 25 mg/L) could slightly facilitate the Pb(II) or PNP adsorption. By comparison with single adsorption system, new adsorption pathways might exist in binary adsorption system. The complex formed between hydroxyl of PNP and Pb(II) might directly formed a complexing-bridging structure. In addition, the complexation might also occur between the adsorbed PNP and free Pb(II) as well as the adsorbed Pb(II) and free PNP [65].

Thus, the increased adsorption of PNP and Pb(II) at their low concentration was dominated by the complexing-bridging mechanism. While at high concentration of Pb(II) and PNP, the great competition between them for interaction with the adsorbent suppressed both of their adsorption, as presented in Fig. 6.

3.5. Desorption of adsorbate from N-Fe/OMC and their reuse

The Pb(II)-loaded (or PNP-loaded) adsorbent could be desorbed with 10 mL 20% acetone solution (or 0.2 mol/L NaOH solution), and then the desorbed materials were reused for Pb(II) or PNP removal. The result was presented in Fig. S-10. It is clear that they could keep above 75.5% for Pb(II) and 83.2% for PNP of its original Pb(II) and PNP removal capabilities, respectively, after being desorbed for four times. Therefore, these recovered N-Fe/OMC could be reutilized for Pb(II) and PNP removal from water, which could reduce the operation cost in a real environmental application.

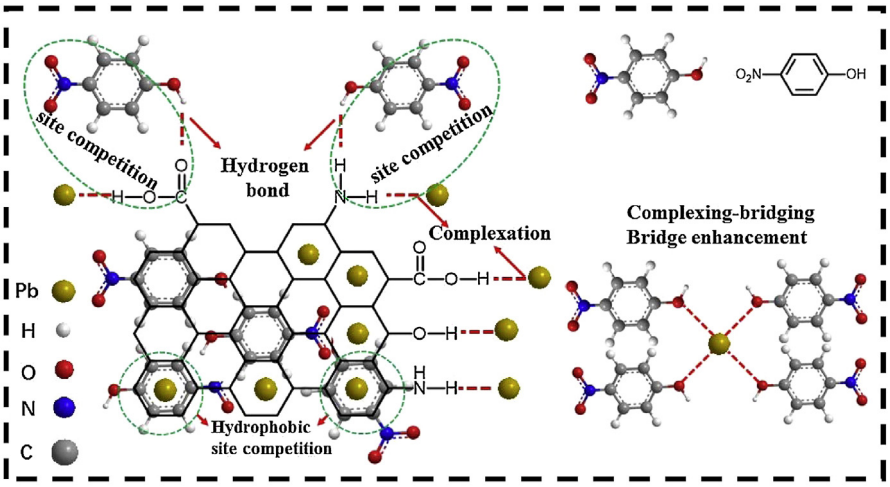

Fig. 6. Schematic for the synergic mechanisms behind coadsorption of Pb(II) and PNP on N-Fe/OMC.

3.6. Application of N-Fe/OMC to real water samples

N-Fe/OMC was used to treat real samples including tap water and landfill leachate to investigate its practical application. The landfill leachate samples were acquired from Heimifeng Refuse Landfill (Changsha, China). The corresponding results were listed in Table S-3. It was found that the adsorption capacity for PNP in tap water was slightly lower than ultrapure water, while the adsorption capacity for PNP in tap water was higher than landfill leachate. The low removal performance in landfill leachate might be explained by that the organic components possessing similar physicochemical properties with PNP would compete with PNP for the adsorption sites on N-Fe/OMC in landfill leachate [66]. Therefore, the PNP adsorption had been diminished. As for Pb(II), the removal performance in tap water and landfill leachate were slightly lower than ultrapure water due to that there may existed many common cations including Na^+, K^+, Ca^{2+} and Mg^{2+} in the former two samples. These cations may occupy the adsorption sites of N-Fe/OMC [5]. The Pb(II) uptake amount in landfill leachate was a little higher than tap water because of plentiful organic matters existing in landfill leachate, such as humic acid and phenolic organics which chelated with Pb(II), and thus improved Pb(II) adsorption [67].

4. Conclusions

In the present study, nitrogen-functionalized magnetic ordered mesoporous carbon (N-Fe/OMC) was synthesized and used to remove Pb(II) and PNP contamination from water. The adsorption mechanism of Pb(II) and/or PNP onto N-Fe/OMC was investigated by different models. N-Fe/OMC contained both hydrophobic and hydrophilic sites, and exhibited excellent adsorption of Pb(II) and PNP. The results of batch adsorption tests showed that site recognition, bridge enhancement and site competition were the predominant adsorption mechanisms. Furthermore, N-Fe/OMC might offer an effective treatment to remove nitroaromatic compounds and heavy metals by in-situ regeneration and reuse.

Acknowledgments

The study was financially supported by the National Natural Science Foundation of China (51579096, 51222805, 51521006 and 51409024), the National Program for Support of Top-Notch Young Professionals of China (2012), the Program for New Century Excellent Talents in University from the Ministry of Education of China (NCET-11-0129), the Scientific Research Fund of Hunan Provincial Education Department(13C1082).

Appendix A. Supplementary data

Supplementary data associated with this article can be found, in the online version, at http://dx.doi.org/10.1016/j.jhazmat.2017.03.031.

References

[1] J. Shen, C. Feng, Y. Zhang, F. Jia, X. Sun, J. Li, W. Han, L. Wang, M. Yang, Bioelectrochemical system for recalcitrant *p*-nitrophenol removal, J. Hazard. Mater. 209–210 (2012) 516–519.
[2] K.R. Thines, E.C. Abdullah, N.M. Mubarak, M. Ruthiraan, Synthesis of magnetic biochar from agricultural waste biomass to enhancing route for waste water and polymer application: a review, Renew. Sustain. Energy Rev. 67 (2017) 257–276.
[3] N. Arancibia-Miranda, S.E. Baltazar, A. García, D. Muñoz-Lira, P. Sepúlveda, M.A. Rubio, D. Altbir, Nanoscale zero valent supported by zeolite and montmorillonite: template effect of the removal of lead ion from an aqueous solution, J. Hazard. Mater. 301 (2016) 371–380.
[4] Y. Zhou, L. Tang, G. Zeng, C. Zhang, Y. Zhang, X. Xie, Current progress in biosensors for heavy metal ions based on DNAzymes/DNA molecules functionalized nanostructures: a review, Sens. Actuators B: Chem. 223 (2016) 280–294.
[5] A. Kundu, B. Sengupta, M.A. Hashim, J.N. Sahu, N.M. Mubarak, G. Redzwan, Optimization of the process variables in production of activated carbon by microwave heating, RSC Adv. 5 (2015) 35899–35908.
[6] N.M. Mubarak, J.N. Sahu, E.C. Abdullah, N.S. Jayakumar, Plam oil empty fruit bunch based magnetic biochar composite comparison for synthesis by microwave-assisted and conventional heating, J. Anal. Appl. Pyrolysis 120 (2016) 521–528.
[7] G. Yang, L. Tang, G. Zeng, Y. Cai, J. Tang, Y. Pang, Y. Zhou, Y. Liu, J. Wang, S. Zhang, Simultaneous removal of lead and phenol contamination from water by nitrogen-functionalized magnetic ordered mesoporous carbon, Chem. Eng. J. 259 (2015) 854–864.
[8] T. Chen, F. Liu, C. Ling, J. Gao, C. Xu, L. Li, A. Li, Insight into highly efficient coremoval of copper and p-nitrophenol by a newly synthesized polyamine chelating resin from aqueous media: competition and enhancement effect upon site recognition, Environ. Sci. Technol. 47 (2013) 13652–13660.
[9] L. Fu, F. Liu, M. Yan, X. Tao, L. Chen, A. Li, C. Shuang, L. Yan, High-efficient technique to simultaneous removal of Cu(II), Ni(II) and tannic acid with magnetic resins: complex mechanism behind integrative application, Chem. Eng. J. 263 (2015) 83–91.
[10] M.N. Noraini, E.C. Abdullah, R. Othman, N.M. Mubarak, Single-route synthesis of magnetic biochar from sugarcane bagasse by microwave-assisted pyrolysis, Mater. Lett. 184 (2016) 315–319.
[11] P. Guo, L. Tang, J. Tang, G. Zeng, B. Huang, H. Dong, Y. Zhang, Y. Zhou, Y. Deng, L. Ma, Catalytic reduction-adsorption for removal of p-nitrophenol and its conversion p-aminophenol from water by gold nanoparticles supported on oxidized mesoporous carbon, J. Colloid Interface Sci. 469 (2016) 78–85.
[12] K.R. Thines, E.C. Abdullah, N.M. Mubarak, M. Ruthiraan, In-situ polymerization of magnetic biochar-polypyrrole composite: a novel application in supercapacitor, Biomass Bioenergy 98 (2017) 95–111.

[13] P. Liu, C.J. Ptacek, D.W. Blowes, R.C. Landis, Mechanisms of mercury removal by biochars produced from different feedstocks determined using X-ray absorption spectroscopy, J. Hazard. Mater. 308 (2016) 233–242.
[14] C. Shan, Z. Ma, M. Tong, Efficient removal of free and nitrilotriacetic acid complexed Cd(II) from water by poly(1-vinylimidazole)-grafted Fe_3O_4@SiO_2 magnetic nanoparticles, J. Hazard. Mater. 299 (2015) 479–485.
[15] K. Ortiz-Martínez, P. Reddy, W.A. Cabrera-Lafaurie, F.R. Román, A.J. Hernández-Maldonado, Single and multi-component adsorptive removal of bisphenol A and 2,4-dichlorophenol from aqueous solutions with transition metal modified inorganic-organic pillared clay composites: effect of pH and presence of humic acid, J. Hazard. Mater. 312 (2016) 262–271.
[16] N.M. Mubarak, A. Kundu, J.N. Sahu, E.C. Abdullah, N.S. Jayakumar, Synthesis of palm oil empty fruit bunch magnetic pyrolytic char impregnating with $FeCl_3$ by microwave heating technique, Biomass Bioenergy 61 (2014) 265–275.
[17] M. Ruthiraan, E.C. Abdullah, N.M. Mubarak, K.R. Thines, New generation of magnetic microporus material for enhancing route for methylene blue removal from waste water, J. Environ. Biotechnol. Res. 6 (2017) 105–116.
[18] L. Tang, C. Ye, G. Yang, Y. Liu, G. Zeng, Y. Zhou, S. Li, J. Wang, S. Zhang, Y. Fang, Cobalt nanoparticles-embedded magnetic ordered mesoporous carbon for highly effective adsorption of rhodamine B, Appl. Surf. Sci. 314 (2014) 746–753.
[19] A. Chen, G. Zeng, G. Chen, J. Fan, Z. Zou, L. Hui, X. Hu, L. Fei, Simultaneous cadmium removal and 2,4-dichlorophenol degradation from aqueous solutions by phanerochaete chrysosporium, Appl. Microbiol. Biotechnol. 91 (2011) 811–821.
[20] A. Ely, M. Baudu, J.P. Basly, Copper and nitrophenol pollutants removal by Na-montmorillonite/alginate microcapsules, J. Hazard. Mater. 171 (2009) 405–409.
[21] A. Ely, M. Baudu, J.P. Basly, Copper and nitrophenol removal by low cost alginate/Mauritanian clay composite beads, Chem. Eng. J. 178 (2011) 168–174.
[22] M. Tripathi, N.M. Mubarak, J.N. Sahu, P. Ganesan, Overview on synthesis of magnetic bio char from discarded agricultural biomass, Handb. Compos. Renew. Mater. Struct. Chem. 1 (2016) 435.
[23] K.R. Thines, E.C. Abdullah, N.M. Mubarak, M. Ruthiraan, In-situ polymerization of magnetic biochar e polypyrrole composite: a novel application in supercapacitor, Biomass Bioenergy 98 (2017) 95–111.
[24] Z. Wu, X. Yuan, H. Zhong, H. Wang, G. Zeng, X. Chen, H. Wang, L. Zhang, J. Shao, Enhanced adsorptive removal of p-nitrophenol from water by aluminum metal-organic framework/reduced graphene oxide composite, Sci. Rep. 6 (2016) 25638.
[25] L. Zhou, L. Ji, P.C. Ma, Y. Shao, Z. He, W. Gao, Y. Li, Development of carbon nanotubes/$CoFe_2O_4$ magnetic hybrid material for removal of tetrabromobisphenol A and Pb(II), J. Hazard. Mater. 265 (2014) 104–114.
[26] H. Gao, Y. Sun, J. Zhou, X. Rong, H. Duan, Mussel-inspired synthesis of polydopamine-functionalized graphene hydrogel as reusable adsorbents for water purification, ACS Appl. Mater. Interfaces 5 (2013) 425–432.
[27] J. Lee, J. Kim, T. Hyeon, Recent progress in the synthesis of porous carbon materials, Adv. Mater. 18 (2006) 2073–2094.
[28] Z. Wu, D. Zhao, Ordered mesoporous materials as adsorbents, Chem. Commun. 47 (2011) 3332–3338.
[29] M. Barczak, K. Michalak-Zwierz, K. Gdula, K. Tyszczuk-Rotko, R. Dobrowolski, A. Dąbrowski, Ordered mesoporous carbons as effective sorbents for removal of heavy metal ions, Microporous Mesoporous Mater. 211 (2015) 162–173.
[30] Q. Bao, H. Zhang, J.X. Yang, S. Wang, D.Y. Tang, R. Jose, S. Ramakrishna, C.T. Lim, K.P. Loh, Ultrafast photonics: graphene-polymer nanofiber membrane for ultrafast photonics, Adv. Funct. Mater. 20 (2010) 782–791.
[31] Z. Wu, P.A. Webley, D. Zhao, Comprehensive study of pore evolution, mesostructural stability, and simultaneous surface functionalization of ordered mesoporous carbon (FDU-15) by wet oxidation as a promising adsorbent, Langmuir 26 (2010) 10277–10286.
[32] C. Tian, Selective adsorption behavior of Cu(II) and Cr(VI) heavy metal ions by functionalized ordered mesoporous carbon, Acta Physicochim. Sin. 26 (2010) 3249–3256.
[33] G. Zeng, Y. Liu, L. Tang, G. Yang, Y. Pang, Z. Yi, Y. Zhou, L. Zhen, M. Li, M. Lai, Enhancement of Cd(II) adsorption by polyacrylic acid modified magnetic mesoporous carbon, Chem. Eng. J. 259 (2015) 153–160.
[34] Y. Zhou, L. Tang, G. Yang, G. Zeng, Y. Deng, B. Huang, Y. Cai, J. Tang, J. Wang, Y. Wu, Phosphorus-doped ordered mesoporous carbons embedded with Pd/Fe bimetal nanoparticles for the dechlorination of 2,4-dichlorophenol, Catal. Sci. Technol. 6 (2015) 1930–1939.
[35] Y. Zhou, L. Tang, G. Zeng, J. Chen, Y. Cai, Y. Zhang, G. Yang, Y. Liu, C. Zhang, W. Tang, Mesoporous carbon nitride based biosensor for highly sensitive and selective analysis of phenol and catechol in compost bioremediation, Biosens. Bioelectron. 61C (2014) 519–525.
[36] Y. Liu, Z. Zeng, G. Zeng, L. Tang, Y. Pang, L. Zhen, C. Liu, X. Lei, M. Wu, P. Ren, Immobilization of laccase on magnetic bimodal mesoporous carbon and the application in the removal of phenolic compounds, Bioresour. Technol. 115 (2011) 21–26.
[37] L. Tang, Y. Zhou, G. Zeng, Z. Li, Y. Liu, Y. Zhang, G. Chen, G. Yang, X. Lei, M. Wu, A tyrosinase biosensor based on ordered mesoporous carbon-Au/L-lysine/Au nanoparticles for simultaneous determination of hydroquinone and catechol, Analyst 138 (2013) 3552–3560.
[38] Y. Zhou, L. Tang, G. Zeng, Z. Chen, X. Xia, Y. Liu, J. Wang, T. Jing, Z. Yi, Y. Deng, Label free detection of lead using impedimetric sensor based on ordered mesoporous carbon–gold nanoparticles and DNAzyme catalytic beacons, Talanta 146 (2015) 641–647.
[39] X. Wang, P. Liu, Y. Tian, L. Zang, Novel synthesis of Fe-containing mesoporous carbons and their release of ibuprofen, Microporous Mesoporous Mater. 145 (2011) 98–103.
[40] Z. Ioannou, J. Simitzis, Adsorption kinetics of phenol and 3-nitrophenol from aqueous solutions on conventional and novel carbons, J. Hazard. Mater. 171 (2009) 954–964.
[41] T.R. Bastami, M.H. Entezari, Activated carbon from carrot dross combined with magnetite nanoparticles for the efficient removal of p-nitrophenol from aqueous solution, Chem. Eng. J. 210 (2012) 510–519.
[42] C. Moreno-Castilla, Adsorption of organic molecules from aqueous solutions on carbon materials, Carbon 42 (2004) 83–94.
[43] S. Zhang, Preparation and application of amorphous Fe-Ti bimetal oxides for arsenic removal, RSC Adv. 5 (2015) 89545–89551.
[44] S. Nasirimoghaddam, S. Zeinali, S. Sabbaghi, Chitosan coated magnetic nanoparticles as nano-adsorbent for efficient removal of mercury contents from industrial aqueous and oily samples, J. Ind. Eng. Chem. 27 (2015) 79–87.
[45] W. Guo, X. Meng, L. Yan, N. Liang, Z. Hu, C. Rui, M. Meng, W. Yun, J. Han, L. Min, Synthesis and application of 8-hydroxyquinoline modified magnetic mesoporous carbon for adsorption of multivariate metal ions from aqueous solutions, J. Ind. Eng. Chem. 21 (2014) 340–349.
[46] X.J. Hu, J.S. Wang, Y.G. Liu, X. Li, G.M. Zeng, Z.L. Bao, X.X. Zeng, A.W. Chen, F. Long, Adsorption of chromium (VI) by ethylenediamine-modified cross-linked magnetic chitosan resin: isotherms, kinetics and thermodynamics, J. Hazard. Mater. 185 (2010) 306–314.
[47] R. Djeribi, O. Hamdaoui, Sorption of copper(II) from aqueous solutions by cedar sawdust and crushed brick, Desalination 225 (2008) 95–112.
[48] Z. Lu, Y. Liu, S. Liu, Y. Yin, G. Zeng, X. Tan, H. Xi, X. Hu, L. Jiang, D. Yang, Investigation of the adsorption-reduction mechanisms of hexavalent chromium by ramie biochars of different pyrolytic temperatures, Bioresour. Technol. 218 (2016) 351–359.
[49] Y.S. Ho, A.E. Ofomaja, Kinetics and thermodynamics of lead ion sorption on palm kernel fibre from aqueous solution, Process Biochem. 40 (2005) 3455–3461.
[50] J. Aguilar-Carrillo, F. Garrido, L. Barrios, M.T. García-González, Sorption of As, Cd and Tl as influenced by industrial by-products applied to an acidic soil: equilibrium and kinetic experiments, Chemosphere 65 (2006) 2377–2387.
[51] M.H. Dehghani, M. Mostofi, M. Alimohammadi, G. Mckay, K. Yetilmezsoy, A.B. Albadarin, B. Heibati, M. Alghouti, N.M. Mubarak, J.N. Sahu, High-performance removal of toxic phenol by single-walled and multi-walled carbon nanotubes: kinetics, adsorption, mechanism and optimization studies, J. Ind. Eng. Chem. 35 (2015) 63–74.
[52] G. Adomian, A review and of the decomposition method some recent results for nonlinear equations, Math. Comput. Modell. 13 (1990) 17–43.
[53] H. Fatoorehchi, H. Abolghasemi, Approximating the minimum reflux ratio of multicomponent distillation columns based on the Adomian decomposition method, J. Taiwan Inst. Chem. Eng. 45 (2014) 880–886.
[54] H. Fatoorehchi, H. Abolghasemi, R. Rach, A new parametric algorithm for isothermal flash calculations by the Adomian decomposition of Michaelis–Menten type nonlinearities, Fluid Phase Equilib. 395 (2015) 44–50.
[55] G. Adomian, R. Rach, Algebraic computation and the decomposition method, Kybernetes 15 (1986) 33–37.
[56] D. Reichenberg, Properties of ion-exchange resins in relation to their structure. III. kinetics of exchange, J. Am. Chem. Soc. 75 (1953) 589–597.
[57] M.W. Yap, N.M. Mubarak, J.N. Sahu, E.C. Abdullah, Microwave induced synthesis of magnetic biochar from agricultural biomass for removal of lead and cadmium from wastewater, J. Ind. Eng. Chem. 45 (2016) 287–295.
[58] K.R. Hall, L.C. Eagleton, A. Acrivos, T. Vermeulen, Pore- and solid-diffusion kinetics in fixed-bed adsorption under constant-pattern conditions, Ind. Eng. Chem. Fundam. 5 (1966) 587–594.
[59] G.D. Halsey, The role of surface heterogeneity in adsorption, Adv. Catal. 4 (1952) 259–269.
[60] G. Mckay, A. Mesdaghinia, S. Nasseri, M. Hadi, M.S. Aminabad, Optimum isotherms of dyes sorption by activated carbon: fractional theoretical capacity & error analysis, Chem. Eng. J. 251 (2014) 236–247.
[61] S.I. El, L. Erdei, J.H. Kim, H.K. Shon, Adsorption and photocatalytic degradation of methylene blue over hydrogen-titanate nanofibres produced by a peroxide method, Water Res. 47 (2013) 4115–4125.
[62] B. Kiran, A. Kaushik, Chromium binding capacity of Lyngbya putealis exopolysaccharides, Biochem. Eng. J. 38 (2008) 47–54.
[63] V.K. Gupta, S. Agarwal, T.A. Saleh, Chromium removal by combining the magnetic properties of iron oxide with adsorption properties of carbon nanotubes, Water Res. 45 (2011) 2207–2212.
[64] G.C. Chen, X.Q. Shan, Y.S. Wang, B. Wen, Z.G. Pei, Y.N. Xie, T. Liu, J.J. Pignatello, Adsorption of 2,4,6-trichlorophenol by multi-walled carbon nanotubes as affected by Cu(II), Water Res. 43 (2009) 2409–2418.
[65] Q.S. Liu, Z. Tong, W. Peng, J.P. Jiang, L. Nan, Adsorption isotherm, kinetic and mechanism studies of some substituted phenols on activated carbon fibers, Chem. Eng. J. 157 (2010) 348–356.
[66] J. Wang, J. Pan, Y. Yin, R. Wu, X. Dai, J. Dai, L. Gao, H. Ou, Thermo-responsive and magnetic molecularly imprinted Fe_3O_4@carbon nanospheres for selective adsorption and controlled release of 2,4,5-trichlorophenol, J. Ind. Eng. Chem. 25 (2014) 321–328.
[67] M.A. Barakat, R. Kumar, Synthesis and characterization of porous magnetic silica composite for the removal of heavy metals from aqueous solution, J. Ind. Eng. Chem. 23 (2014) 93–99.